Numerical simulation of EMC tests for compliance

Comparison of 3-D Direct Microwave Imaging Algorithms Applied to Brain Stroke Follow-up

1st Alex R. Masaquiza-Caiza
Dept. of Elec. and Telecomm.
Politecnico di Torino
Torino, Corso Duca degli Abruzzi 24
alex.masaquiza@polito.it

2nd David O. Rodriguez-Duarte
Dept. of Elec. and Telecomm.
Politecnico di Torino
Torino, Corso Duca degli Abruzzi 24
david.rodriguez@polito.it

3rd Martina Gugliermino
Dept. of Elec. and Telecomm.
Politecnico di Torino
Torino, Corso Duca degli Abruzzi 24
martina.gugliermino@polito.it

4th Francesca Vipiana
Dept. of Elec. and Telecomm.
Politecnico di Torino
Torino, Corso Duca degli Abruzzi 24
francesca.vipiana@polito.it

***Abstract*—This paper presents features and performance comparison of two non-iterative inversion approaches used for microwave-imaging-based monitoring of after-onset stroke infarct migrations, utilizing 3-D realistic full-wave twin numerical experiments that mimic a controlled progressing hemorrhage scenario. Specifically, it considers two well-established approaches with the potential for real-time operation and low computational demand: a tomographic approach based on a truncated singular value decomposition and the Born approximation, a frequency-domain method; and the Delay-Multiply-And-Sum, a time-domain method. The setup and implications of both approaches are discussed, and their performance is assessed using various metrics, which indicate the fidelity of the retrievals.**

***Index Terms*—Biomedical microwave imaging, brain stroke, delay multiply and sum, inverse scattering, confocal microwave imaging, truncated singular value decomposition.**

I. Introduction

Stroke is a neurological disorder characterized by a disruption in the regular supply of rich-oxygen blood to the brain, derived either from a clot provoking an ischemia (IS) or from bleeding or ruptured vessels causing an intracranial hemorrhage (ICH) [1]. The clinical diagnosis of strokes strongly relies on well-established imaging technologies, including magnetic resonance imaging (MRI) and computed tomography (CT) [2], [3], which provide reliable and accurate images that support the identification of the infarct region, being key for planning interventions. However, the clinical pathway still lacks instruments for post-acute stroke follow-up. To overcome this limitation, microwave imaging (MWI)-based solutions have emerged as a complementary approach, enabling the development of compact, portable, cost-effective, and non-invasive diagnostic systems [4].

This work was supported in part by the Agritech National Research Center and received funding from the European Union Next-GenerationEU (PIANO NAZIONALE DI RIPRESA E RESILIENZA (PNRR) – MISSIONE 4 COMPONENTE 2, INVESTIMENTO 1.4 – D.D. 1032 17/06/2022, CN00000022), and by the research project "3BAtwin" funded by Horizon EU FP (101159623), and is part of the research project "MedWaveImage - Microwave imaging technology transfer to innovate the medical sector", funded by Interreg Central Europe (CE0200670) This manuscript reflects only the authors' views and opinions, neither the European Union nor the European Commission can be considered responsible for them.

At microwave frequencies, head tissues exhibit different electromagnetic properties — permittivity and conductivity — which contrast with those of the stroke lesion, allowing for the retrieval of dielectric contrast maps using inverse scattering imaging algorithms. In this work, two representative non-iterative inversion strategies for microwave-based monitoring of stroke evolution are compared: a tomographic approach based on truncated singular value decomposition (TSVD) with the Born approximation, and a confocal method relying on delay-multiply-and-sum (DMAS) beamforming. Both algorithms are assessed through 3-D realistic full-wave numerical experiments that emulate progressive hemorrhagic scenarios. Their performance is analyzed using multiple quantitative metrics to highlight strengths, limitations, and potential suitability for real-time, low-cost monitoring applications in clinical practice.

II. Mathematical Formulation

By definition, the MWI is an inverse ill-posed and non-linear problem that retrieves a spatially distributed map, i.e., an image, of a dielectric contrast variation, $\Delta\chi$, within the Domain of Interest (DoI), taking as input the differential scattering samples, $\Delta S = S_{t_1} - S_{t_2}$, measured outside of DoI at two different time instants, t_1 and t_2. In the specific case of the stroke follow-up, the retrieved images illustrate the progression of the infarct zone between two different examination instances. To address this problem, there are two primary approaches: the direct, non-iterative approach and the iterative approach. In the first case, the algorithm resolves the problem in one shot, which is very convenient when working with applications that require instantaneous results. On the other hand, the iterative methods address the inversion as an

iterative optimization problem, requiring more computational resources and resolving time.

Considering the real-time operational needs that may imply the stroke follow-up, this work adopts direct approaches as study subjects. Specifically, a single-frequency multi-static configuration is employed in the TSVD case, while a mono-static multi-frequency configuration is employed in the DMAS case to generate time-domain responses via inverse Fourier transform. In both approaches, a homogeneous human head model is considered to build the inversion kernel.

A. Born Approximation and Truncated Singular Value Decomposition

Assuming a small and concentrated $\Delta\chi$, a reasonable assumption given the nature of a stroke monitoring scenario, we linearize the imaging operator using the Born approximation. Then, we regularize and invert the scattering problem using the TSVD approach as stated in:

$$\Delta\chi = \sum_{n=1}^{T} \frac{1}{\sigma_n} \langle \Delta S, u_n \rangle \, v_n, \tag{1}$$

where σ_n, u_n, and v_n are the n-th singular value, right, and left singular vectors, respectively, obtained via the singular value decomposition (SVD) of the discretized operator. In (1), the truncation index T acts as a regularizer [5]. It is worth mentioning that the singular system is computed offline, while the contrast retrieval, i.e., the inversion, is performed in real-time, taking only a few seconds on a standard laptop. Further details might be found in [6].

B. Delay-Multiply-And-Sum

DMAS is a fast and robust beamforming algorithm used in microwave imaging [7], [8]. Confocal-based algorithms image by applying geometrically computed delays to the collected time-domain signals to generate intensity maps that represent the contrast in the dielectric properties of scatterers in the background medium.

To isolate the contrast variation, a differential approach is adopted [9], where the back-scatterer response of the i-antenna taken in two consecutive time instants t_1 and t_2 $\mathcal{M}_i$, is given as:

$$\Delta\mathcal{M}_i = \mathcal{M}_i^{t_1} - \mathcal{M}_i^{t_2}, \quad i = 1, 2, ..., N, \tag{2}$$

In a mono-static configuration with N antennas, the intensity distribution $I(r)$ at each focal point r of the DoI is calculated as:

$$I(r) = \sum_{i=1}^{N-1} \sum_{j=i+1}^{N} \Delta\mathcal{M}_i(\tau_i(r)) \Delta\mathcal{M}_j(\tau_j(r)), \tag{3}$$

where $\tau_n(r) = 2\|r - r_n\|/v$ is the delay compensation for the signal travel from the phase center of the n-transmitter r_n to r, $n \in i, j$, and v, the signal velocity in the background medium.

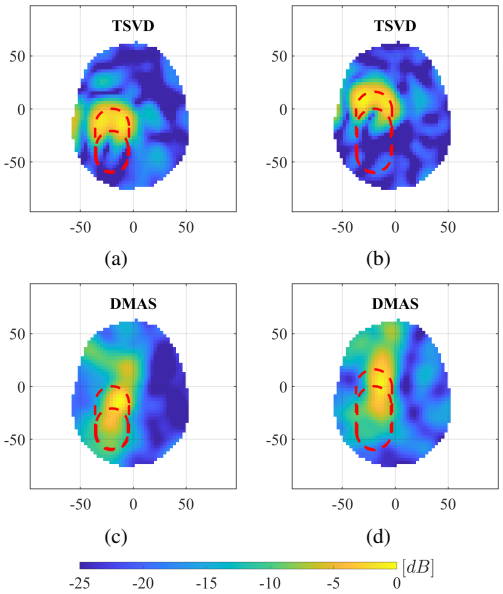

Fig. 1. Monitoring of ICH evolution. Normalized transversal cross-views cut in the middle of the stroke region of the 3D retrieved maps using: (a-b) TSVD, (c-d) DMAS. (left-column) variation between 20 and 40 cm^3, and (right-column) between 40 and 60 cm^3. The red dotted contours indicate the stroke shape. Dimensions in [mm].

III. Numerical Results

Synthetic scattering data are generated using a high-fidelity frequency-based full-wave electromagnetic solver [6], [10]. The antenna system consists of twenty-two elements operating around 1 GHz and arranged in two concentric rings surrounding a multi-tissue human head model. The scattering parameters collected from each antenna pair are organized in a matrix form $S_{m,n,k}$ where m and n are the indices of the antennas, and k corresponds to the frequency index. The frequency range spans from 0.8 GHz up to 2 GHz. Detailed information about the anthropomorphic head model, its internal tissue structures, and the corresponding electromagnetic properties can be found in [11], [12]. As reference, the properties of the tissues included in the model at 1 GHz, skin, fat, bone, cerebrospinal fluid (CSF), white matter, gray matter, and hemorrhagic stroke, have a relative permittivity of approximately 40.27, 5.82, 14.02, 67.89, 39.73, 50.27, and 65, and conductivity of approximately 0.82, 0.045, 0.13, 2.24, 0.76, 1.06, and 1.5 S/m, respectively. The stroke lesion is modeled as a capsule-shaped hemorrhage, progressively increasing in volume along the transverse plane from 20 cm^3 to 40 cm^3, and up to 60 cm^3, as in [6].

The reconstructions for both algorithms are shown in Figs. 1 and 2, transversal slices view and 3-D view, respectively. These results confirm the feasibility of MWI in monitoring stroke evolution, signaling the target region, even when using a distorted homogeneous kernel. Note that this is not a trivial assumption, considering that patient-specific tissue structures are often unavailable in many clinical scenarios.

To evaluate reconstruction performance, binary and full-

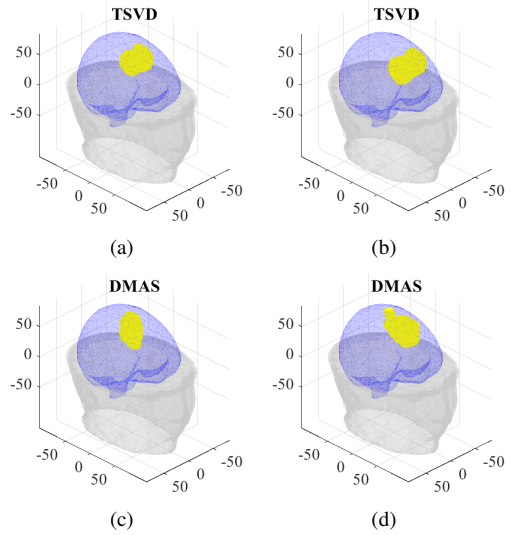

Fig. 2. Monitoring of ICH evolution. Normalized 3-D reconstructions using: (a-b) TSVD, (c-d) DMAS. (left-column) variation between 20 and 40 cm^3, and (right-column) between 40 and 60 cm^3. Dimensions in [mm].

contrast metrics are used. In this context, metrics refer to numerical indicators that quantify the similarity between the reconstructed image and the corresponding ground truth. For the former, a reference binary ground truth is compared with a binarized version of the volumetric reconstruction, where points above -5 dB are thresholded to 1, and 0 otherwise. In contrast, the full-contrast ones use the normalized volumetric reconstruction alongside the ground truth. First, the intersection over union (IoU) and dice similarity coefficient (DSC) [13]. These evaluate the fraction of overlapping region between the reconstruction and the ground truth, relative to the union, as well as the total size of the areas, respectively. Moreover, we use two other binary metrics, the size-based metric (S-BM) and the boundary-based metric (B-BM), both proposed in [14], to measure the size correspondence and the distance between the boundaries of the reconstruction and the ground truth, respectively. Regarding the full-contrast one, we use the structural similarity index (SSIM) [15], a full-contrast-based metric, to measure global image similarity with respect to brightness, contrast, and structure. All these metrics are bounded from 0 to 1; no correspondence between the reconstructed image and the ground truth is represented with 0, and full correspondence is represented with 1. B-BM and SSIM metrics evaluate differences between the reconstructions and the ground truth with respect to the complete DoI volume. When target variations are small relative to the total volume, metric sensitivity is reduced. To enhance precision, we additionally analyze these metrics on a partial-volume, which is the region bounded by red-dash lines in Fig. 1 with 50 % extra margin, providing focused metric analysis.

Table I provides a quantitative summary of the reconstructed volumes. The results show that, in general, TSVD achieved higher values in IoU, and DSC, indicating a relatively better overlap between the reconstructed volume/boundaries and the

TABLE I
IMAGING PERFORMANCE METRICS

Method	MWI algorithm	IoU	DSC	S-BM	B-BM	SSIM
Partial volume	TSVD	0.3078	0.4669	0.8381	0.8656	0.3511
	DMAS	0.2644	0.4145	0.8310	0.8254	0.3119
Full volume	TSVD	0.3078	0.4669	0.8381	0.9179	0.8120
	DMAS	0.2644	0.4145	0.8310	0.8967	0.7949

reference evolving stroke regions. DMAS and TSVD have similar performance in S-BM, suggesting precise stroke volume estimation using both algorithms. However, this metric overlooks the consideration of relative position. Finally, B-BM and SSIM have differences between the full- and partial-volume. But consistently indicate that TSVD predicts the stroke evolving better than DMAS. In general, the evaluated metrics are comparable for both algorithms, indicating that they effectively reconstruct the fundamental structural information of the stroke evolution. The MWI algorithms presented in this work can be translated to practical systems, addressing some practical implementation aspects, including but not limited to the use of adequate hardware, a low-noise measurement environment, appropriate signal processing, and calibration, among many others. In real implementations, the noise-free conditions assumed in simulations would be addressed with high signal-to-noise-ratio (SNR) equipment, high-phase stability cables, and adequate antenna isolation from external electromagnetic interferences. For both algorithms, a priori information such as the head anatomy of patients can further improve the quality of MWI reconstructions, and such information, obtained via MRI or CT, is often available in standard post onset-stroke clinical protocols.

IV. Conclusion and Perspectives

This work compares TSVD and DMAS in the context of brain stroke monitoring. Both algorithms successfully localize changes in dielectric properties within the injured brain regions. Approximate models within the inversion kernel introduce a model error that limits reconstruction accuracy; however, they still provide valuable information for clinicians. To quantify the algorithms' performance, a quantitative analysis using biomedical imaging metrics was conducted. The results show that TSVD and DMAS have comparable performance for brain stroke monitoring. For future work, it is planned to extend stroke follow-up by integrating additional a-priori dependent patient information into the inversion kernel of MWI algorithms to reduce artifacts in reconstructions.

References

[1] D. Kuriakose and Z. Xiao, "Pathophysiology and treatment of stroke: present status and future perspectives," *International journal of molecular sciences*, vol. 21, no. 20, p. 7609, 2020.

[2] J. J. Nukovic, V. Opancina, E. Ciceri, M. Muto, N. Zdravkovic, A. Altin, P. Altaysoy, R. Kastelic, D. M. Velazquez Mendivil, J. A. Nukovic, N. V. Markovic, M. Opancina, T. Prodanovic, M. Nukovic, J. Kostic, and N. Prodanovic, "Neuroimaging modalities used for ischemic stroke diagnosis and monitoring," *Medicina*, vol. 59, no. 11, 2023.

[3] K. B. Walsh, "Non-invasive sensor technology for prehospital stroke diagnosis: Current status and future directions," *International Journal of Stroke*, vol. 14, no. 6, pp. 592–602, 2019.

[4] C. Origlia, D. O. Rodriguez-Duarte, J. A. Tobon Vasquez, J.-C. Bolomey, and F. Vipiana, "Review of microwave near-field sensing and imaging devices in medical applications," *Sensors*, vol. 24, no. 14, 2024. [Online]. Available: https://www.mdpi.com/1424-8220/24/14/4515

[5] M. Bertero, P. Boccacci, and C. De Mol, *Introduction to inverse problems in imaging*. CRC press, 2021.

[6] D. O. Rodriguez-Duarte, C. Origlia, J. A. T. Vasquez, R. Scapaticci, L. Crocco, and F. Vipiana, "Experimental assessment of real-time brain stroke monitoring via a microwave imaging scanner," *IEEE Open Journal of Antennas and Propagation*, vol. 3, pp. 824–835, 2022.

[7] G. Matrone, A. S. Savoia, G. Caliano, and G. Magenes, "The delay multiply and sum beamforming algorithm in ultrasound b-mode medical imaging," *IEEE Transactions on Medical Imaging*, vol. 34, no. 4, pp. 940–949, 2015.

[8] M. Mozaffarzadeh, A. Mahloojifar, M. Orooji, S. Adabi, and M. Nasiriavanaki, "Double-stage delay multiply and sum beamforming algorithm: Application to linear-array photoacoustic imaging," *IEEE Transactions on Biomedical Engineering*, vol. 65, no. 1, pp. 31–42, 2018.

[9] S. Mustafa, B. Mohammed, and A. Abbosh, "Novel preprocessing techniques for accurate microwave imaging of human brain," *IEEE Antennas and Wireless Propagation Letters*, vol. 12, pp. 460–463, 2013.

[10] D. O. Rodriguez-Duarte, J. A. T. Vasquez, R. Scapaticci, L. Crocco, and F. Vipiana, "Assessing a microwave imaging system for brain stroke monitoring via high fidelity numerical modelling," *IEEE Journal of Electromagnetics, RF and Microwaves in Medicine and Biology*, vol. 5, no. 3, pp. 238–245, 2021.

[11] C. Origlia, M. Gugliermino, D. O. Rodriguez-Duarte, J. A. Tobon Vasquez, and F. Vipiana, "Anthropomorphic multi-tissue head phantom for microwave imaging devices testing," in *2023 17th European Conference on Antennas and Propagation (EuCAP)*, 2023, pp. 1–4.

[12] "An internet resource for the calculation of the dielectric properties of body tissues in the frequency range 10 Hz - 100 GHz," Available at http://niremf.ifac.cnr.it/tissprop/htmlclie/htmlclie.php.

[13] K. H. Zou, S. K. Warfield, A. Bharatha, C. M. Tempany, M. R. Kaus, S. J. Haker, W. M. Wells III, F. A. Jolesz, and R. Kikinis, "Statistical validation of image segmentation quality based on a spatial overlap index1: scientific reports," *Academic radiology*, vol. 11, no. 2, pp. 178–189, 2004.

[14] F. Xue, L. Guo, A. Bialkowski, and A. M. Abbosh, "Integrated boundary-overlap-size metric for local assessment of deep learning methods in medical microwave imaging," *IEEE Journal of Electromagnetics, RF and Microwaves in Medicine and Biology*, vol. 9, no. 2, pp. 229–239, 2025.

[15] Z. Wang, A. Bovik, H. Sheikh, and E. Simoncelli, "Image quality assessment: from error visibility to structural similarity," *IEEE Transactions on Image Processing*, vol. 13, no. 4, pp. 600–612, 2004.